ACS NANO

www.acsnano.org

ARTICLE

Correlated Structural and Optical Characterization of Hexagonal Boron Nitride

Jordan A. Gusdorff,[‖] Pia Bhatia,[‖] Trey T. Shin, Alexandra Sofia Uy-Tioco, Benjamin N. Sailors, Rachael N. Keneipp, Marija Drndić,* and Lee C. Bassett*

Cite This: *ACS Nano* 2025, 19, 11100−11110

Read Online

ACCESS | Metrics & More | Article Recommendations | Supporting Information

ABSTRACT: **Hexagonal boron nitride (hBN) plays a central role in nanoelectronics and nanophotonics. Moreover, hBN hosts room-temperature quantum emitters and optically addressable spins, making the material promising for quantum sensing and photonics. Despite significant investigation of the optical and structural properties of hBN, the role of contamination at surfaces and interfaces remains unexplored. We prepare hBN samples that are compatible with confocal photoluminescence (PL) microscopy, transmission electron microscopy (TEM), and atomic-force microscopy (AFM), and we use those techniques to quantitatively investigate correlations between fluorescent emission, flake morphology, and surface residue. We find that the microscopy techniques themselves induce changes in hBN's optical activity and residue morphology: PL measurements induce photobleaching, whereas TEM measurements alter surface residue and emission characteristics. We also study the effects of common treatments—annealing and oxygen plasma cleaning—on the structure and optical activity of hBN. The methods can be broadly applied to study two-dimensional materials, and the results illustrate the importance of correlative studies to elucidate factors that influence hBN's structural and optical properties.**

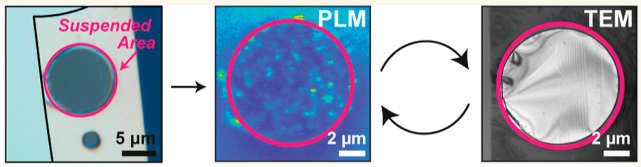

KEYWORDS: *hexagonal boron nitride, quantum emission, photoluminescence microscopy, transmission electron microscopy, multilayer crystal*

Hexagonal boron nitride (hBN) is a van der Waals material with broad utility. As a wide-bandgap semiconductor (∼5.9 eV),[1,2] hBN serves a key role as a dielectric layer in electronic devices.[3−5] In addition, hBN is poised to play a key role in quantum information science, since the material hosts bright quantum emitters at room temperature.[6−9] Some emitters display spin-dependent optical properties and can be utilized as spin qubits.[10−14] However, hBN's quantum emitters are not yet fully understood. Identifying emitters in two-dimensional materials is especially complex because they are sensitive to interfaces[7,15] and other local environmental effects (e.g., defects,[11] strain,[16,17] and contamination[18,19]). Understanding and controlling the properties of hBN, especially at its surface, are therefore crucial to advancing quantum information and photonics applications. Techniques such as photoluminescence (PL) microscopy and scanning electron microscopy (SEM) are commonly employed to characterize hBN. PL provides information about optical properties, including absorption and emission characteristics. For the study of quantum emitters, it provides essential chemical and electronic information via the spectra of electronic and vibronic transitions,[2,7,20] as well as spatial information regarding the emitters' density and brightness.[21] SEM has been used to study surface topography and morphology,[7,8] in addition to activating emission centers in hBN.[6,21,22] More recently, transmission electron microscopy (TEM) has been used as a means of probing quantum emission in hBN, particularly when paired with PL or cathodoluminescence spectroscopy.[19,23] TEMs enable direct observation of material structure down to the atomic level and are generally operated at much higher accelerating voltages than SEMs (∼80−200 vs ∼5−30 kV), opening up a new regime of irradiation conditions to be explored for the possible creation of emitters.[24−26]

While the optical properties and material structure of hBN are often studied separately, few studies have investigated them in parallel. The absence of studies employing both TEM and PL microscopy can be partially attributed to the disparity in scale at which these two techniques operate. Confocal PL

Received: December 6, 2024
Revised: January 31, 2025
Accepted: February 3, 2025
Published: February 21, 2025

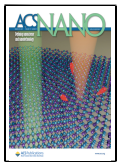

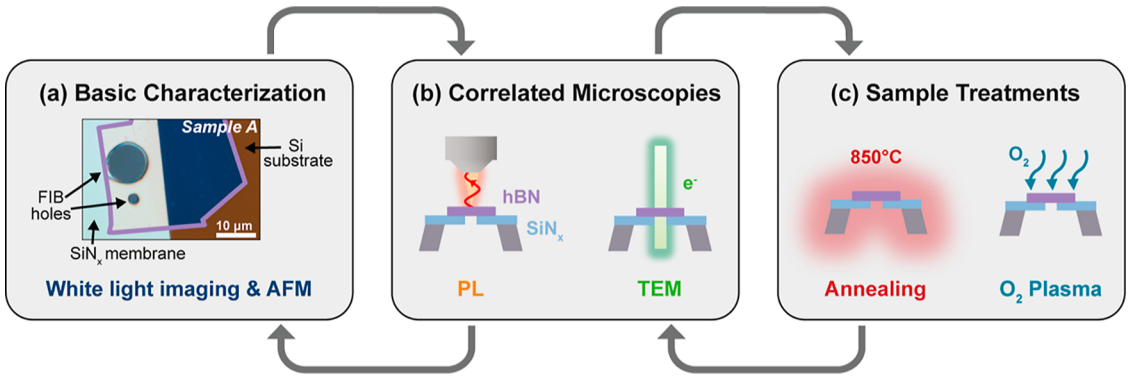

Figure 1. Summary of experimental methods. HBN samples undergo an iterative process that includes basic characterization, correlative PL and TEM measurements, and treatments. (a) All samples are first characterized with white light imaging and AFM. The white light image shows Sample A, a mechanically exfoliated flake of hBN (outlined in purple) suspended over a 10 μm diameter hole milled in a silicon nitride membrane. (b) Basic characterization is followed by PL and/or TEM measurements. The schematics illustrate a cross-sectional view of each correlated microscopy technique. (c) Some samples then receive annealing and/or oxygen plasma treatments. Changes in optical activity and morphology following treatment are analyzed via the correlated microscopies and basic characterization methods.

Table 1. Summary of Sequential Measurements and Treatments

sample	figure	characterization and treatment sequence
A	Figures 1−3 and S4−S6 and S9	AFM → PL → TEM[a]→ PL → TEM → PL → TEM[b]
B	Figures 4 and S7 and S10	AFM → PL → TEM → PL → O_2 plasma (5 m) → AFM → PL → TEM → PL
C	Figures 4 and S8 and S10	AFM → PL → TEM → PL → anneal → PL → TEM → PL → AFM
D	Figures 5 and S11	AFM → PL → O_2 plasma (5 m) → AFM → PL → anneal → PL
E	Figures 5 and S11	AFM → PL → anneal → PL → O_2 plasma (10 m) → AFM → PL
F	Figure S12	AFM → PL → O_2 plasma (10 m) → PL → anneal → PL → AFM

[a]See Figure S9 for further details. [b]EDS measurements taken.

studies in the visible-wavelength range are typically limited by diffraction to a resolution of ∼300 nm, whereas TEM studies can achieve atomic resolution. When used together, these techniques can yield complementary information regarding the structural and chemical composition of fluorescent emitters.

In this work, we combine PL and TEM imaging together with atomic-force microscopy (AFM) to bridge the gap in understanding between hBN's optical properties and material structure. We study changes in optical activity and flake morphology associated with different measurements and treatments, focusing on overall statistical properties of the material rather than investigating individual single-photon emitters with PL or few-atom defects with TEM. To this end, we fabricate custom substrates compatible with both microscopies onto which hBN flakes are transferred with thicknesses ranging from ∼10 to 30 nm. First, we consider the effects of PL and TEM measurements themselves. Using quantitative methods, we show that exposure to the electron beam during TEM imaging induces changes to surface contaminants and that PL imaging induces photobleaching. Subsequently, we study correlated changes in structure and optical activity following annealing and oxygen plasma, treatments commonly applied to hBN.[1,19,27−30] While other studies have focused on improving quantum emission through sample treatments,[6,31,32] we study how these treatments impact hBN's structure and surface contamination, which are then correlated with optical properties. We discuss the implications of this work for understanding and controlling fluorescent emission in hBN, as well as for future investigations of other two-dimensional materials.

RESULTS AND DISCUSSION

Figure 1 summarizes the sample geometry along with the different characterization methods and treatments we explore in this work. We report results for six hBN samples, labeled A through F, each of which received a distinct sequence of measurements and treatments that are summarized in Table 1. The icons representing PL microscopy, TEM, oxygen plasma treatment, and annealing in Figure 1 are also used throughout this manuscript to visually represent the sequence of measurements and treatments performed on each sample. Sample preparation begins by mechanically exfoliating flakes of hBN from bulk crystal (HQ Graphene) and using polydimethylsiloxane (PDMS) viscoelastic stamping to transfer flakes onto 100 × 100 μm^2 silicon nitride (SiN_x) windows. To improve TEM resolution and ensure that PL measurements are not subject to substrate induced effects, hBN flakes are suspended over holes patterned in SiN_x windows via focused ion beam (FIB) milling. A 5- to 10-μm-diameter FIB hole (Figure 1a) provides a sufficiently large region of suspended hBN suitable for both TEM and PL microscopy. Smaller, 1- to 2-μm-diameter FIB holes (Figure 1a) help define the sample orientation and provide an area over which the TEM can initially be aligned.

Flake thickness is another important consideration. Monolayer or few-layer flakes are best for TEM studies at atomic resolution. However, stable single-photon emitters in hBN tend to occur in thicker flakes that are typically at least 30 nm thick.[33,34] Therefore, we utilize flakes of intermediate thickness, ranging from ∼10 to ∼30 nm, to meet the needs of both microscopies. Flakes of the desired thickness are identified by optical contrast prior to transferring and subsequently

https://doi.org/10.1021/acsnano.4c17676
ACS Nano 2025, 19, 11100−11110

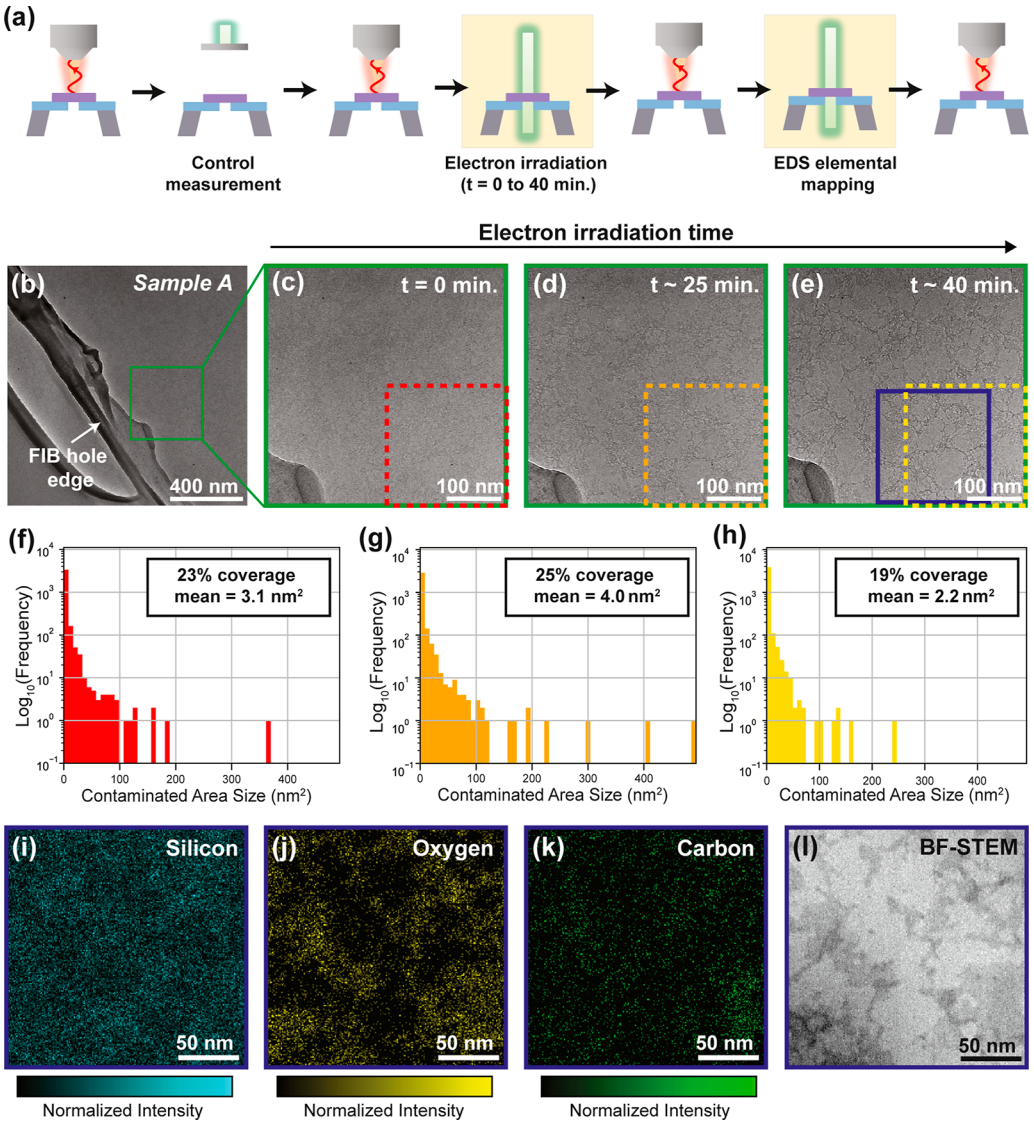

Figure 2. Effect of TEM electron irradiation on hBN contaminants. (a) Schematic depicting the sequence of measurements and treatments performed on Sample A with yellow boxes representing steps included in this figure. (b) Low magnification TEM image of Sample A. The green box denotes the region shown in (c–e). (c) Initial TEM image of a suspended region of hBN. The region boxed in red was analyzed to produce the histogram in panel (f). (d) TEM micrograph of the same region after ~25 min of exposure to the electron beam. The region boxed in orange was analyzed to produce the histogram in panel (g). (e) TEM micrograph of the same region after ~40 min of exposure to the electron beam, illustrating a change in surface contamination morphology. The region boxed in yellow was analyzed to produce the histogram in panel (h). The blue box corresponds to panels (i–l). (i–k) EDS elemental maps taken of Sample A. (l) Bright-field scanning TEM (BF-STEM) micrograph of the same region shown in the elemental maps.

confirmed with AFM (see Tables S1 and S2 and Figures S1–S3 in the Supporting Information).

Effects of PL and TEM Imaging. Figure 2 demonstrates the effect of electron beam irradiation in the TEM on a representative region of Sample A over time. The sample is initially covered with a film of residue, as seen in Figure 2c. However, with prolonged exposure to the electron beam (~20 nA probe current), the residue changes in structure and density. Qualitatively, the residue appears to clump together and diminish over time, resulting in the lacey network of residue shown in Figure 2e after 40 min of irradiation. We quantitatively analyze the residue using an image-processing algorithm to detect regions of contamination and characterize its spatial distribution, as described in Section SIII of the Supporting Information. Figure 2f–h show the contamination area distributions corresponding to each image along with the overall surface coverage. Interestingly, we observe that both the surface coverage and mean area increase slightly over the first 25 min of TEM exposure, and then decrease after 40 min. The overall decrease in contamination coverage and average size between 0 and 40 min of irradiation shows that prolonged exposure to the electron beam has a cleaning effect, while the increase between 0 and 25 min implies that this effect is dose-dependent. It has been shown that hydrocarbons tend to diffuse across the surface of samples toward the electron beam where they are eventually polymerized and fixed in place, often covering features of interest.[35,36] On the other hand, electron irradiation can also remove material through knock-on damage, radiolysis, or charging effects.[37] These competing phenomena may explain the nonmonotonic changes we observe.

The residue shown in Figure 2c–e likely arises from the PDMS polymer used to transfer hBN flakes onto the

https://doi.org/10.1021/acsnano.4c17676
ACS Nano 2025, 19, 11100–11110

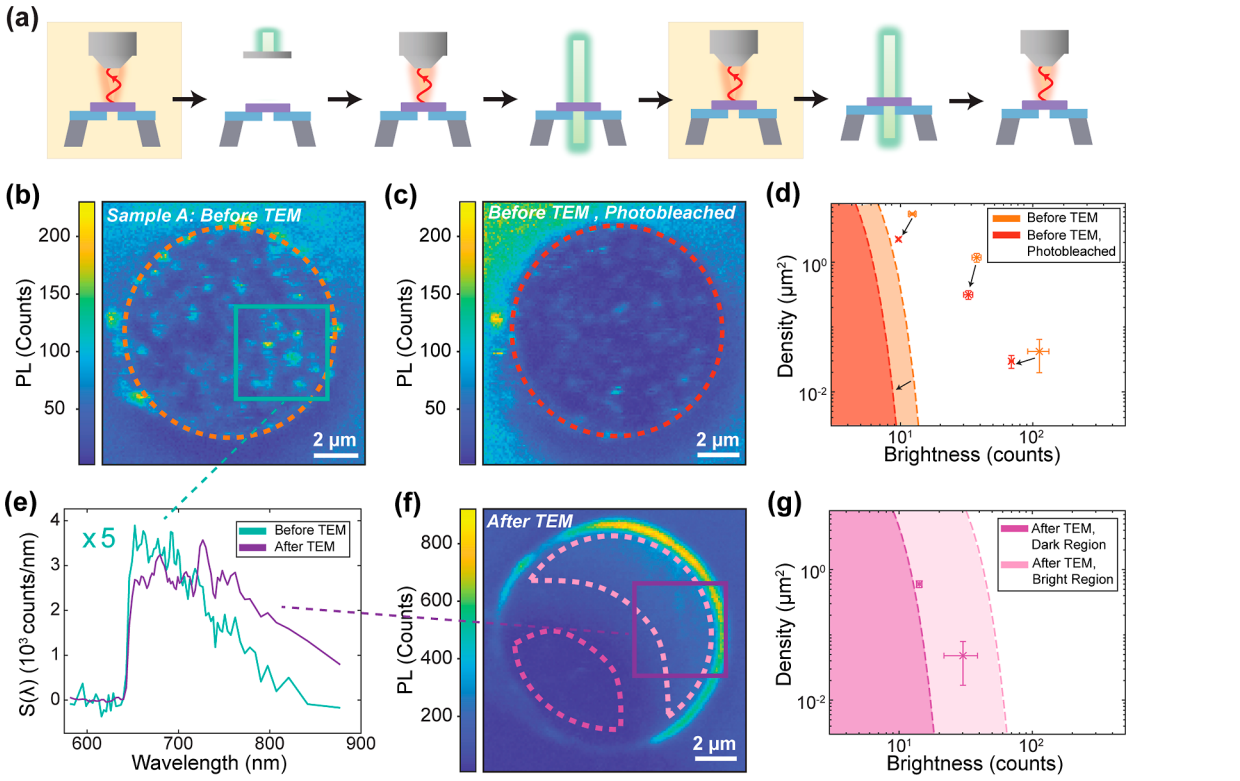

Figure 3. Measurement effects on optical properties. (a) Schematic depicting the sequence of measurements and treatments performed on Sample A with yellow boxes representing steps included in this figure. (b) Initial PL image of Sample A. Orange dashed circle outlines suspended area analyzed in (d). Teal square outlines area of PL spectrum collection. (c) PL image after photobleaching. Red dashed circle outlines area analyzed in (d). (d) Emitter family analysis of Sample A before observations in the TEM. Arrows indicate the likely evolution of the emitter families due to photobleaching. (e) Spatial PL spectra corresponding to the initial PL image (teal curve) and the PL image after TEM measurements (purple curve). (f) PL image after TEM measurements. Light pink and dark pink dashed outlines distinguish the bright and dark regions, respectively, which are analyzed in panel (g). (g) Emitter family analysis after TEM measurements.

substrates. A wide body of literature describes how contamination arising from polymer-assisted transfer techniques of 2D materials is a pervasive issue for the field.[38−41] Energy dispersive X-ray spectroscopy (EDS) maps confirm the presence of silicon, carbon and oxygen species, which is consistent with the chemical composition of PDMS (see Figures 2i−k and S4 in the Supporting Information). Moreover, all three maps appear to be spatially correlated with the contaminated (dark) areas in the corresponding brightfield scanning TEM (BF STEM) image (Figure 2l). In recent related work, we used electron energy loss spectroscopy (EELS) and aberration corrected STEM to study the composition and spatial distribution of surface contamination that results from transfer of hBN using PDMS and poly bis-A carbonate (PC) polymers.[38] We found that both transfer methods yield flakes with significant and comparable residue, underscoring the importance of further research to improve transfer methods and to establish reliable cleaning protocols.

To understand how TEM electron irradiation and associated changes to surface contaminants impact optical activity, Sample A was also studied with confocal PL microscopy before and after TEM imaging. Figure 3 summarizes the results. The first confocal PL image prior to electron irradiation shows bright localized emission (Figure 3b). The 592 nm laser was then rastered over the 12 × 12 μm^2 area at 100 μW for about 20 min, and then at 300 μW for about 2 min. The subsequent PL image (Figure 3c) shows that after prolonged laser exposure, emission is still localized but is substantially dimmer within the suspended region. This phenomenon, known as photobleaching, is ubiquitous to quantum emitters and has been previously observed in hBN.[19] Figure 3d shows the results of a statistical analysis of these data that identifies families of emitters based on their density and brightness (see Breitweiser et al.[21] and Section Methods for details). The results indicate a decrease in emitter density or brightness by a factor of ∼3 following the laser exposure, accompanied by a decrease in the overall PL background. In order to assess the spectral properties of the emitter ensembles, optical spectra were acquired while continuously rastering the confocal spot over the ∼5 × 5 μm rectangular region marked in Figure 3b. The resulting spatially averaged spectrum (teal curve in Figure 3e) is consistent with the typical distribution of visible quantum emitters in these samples.[6,7,9]

After photobleaching, a control measurement was performed to understand how the TEM environment without the electron beam affects optical activity (see Section SV in the Supporting Information for more details). Sample A was then subjected to electron irradiation in the TEM to obtain the data shown in Figure 2c−e (see Figure 3a and Table 1 for the full sequence of measurements), and then returned to the optical microscope. Figure 3f illustrates the dramatic qualitative change in the fluorescence properties following TEM imaging. The overall fluorescent intensity increases by a factor of ∼4, and a bright ring appears at the edges of the suspended region. The upper right portion of the suspended region exhibits diffuse bright emission, whereas the lower left portion—where Sample A was

https://doi.org/10.1021/acsnano.4c17676
ACS Nano 2025, 19, 11100−11110

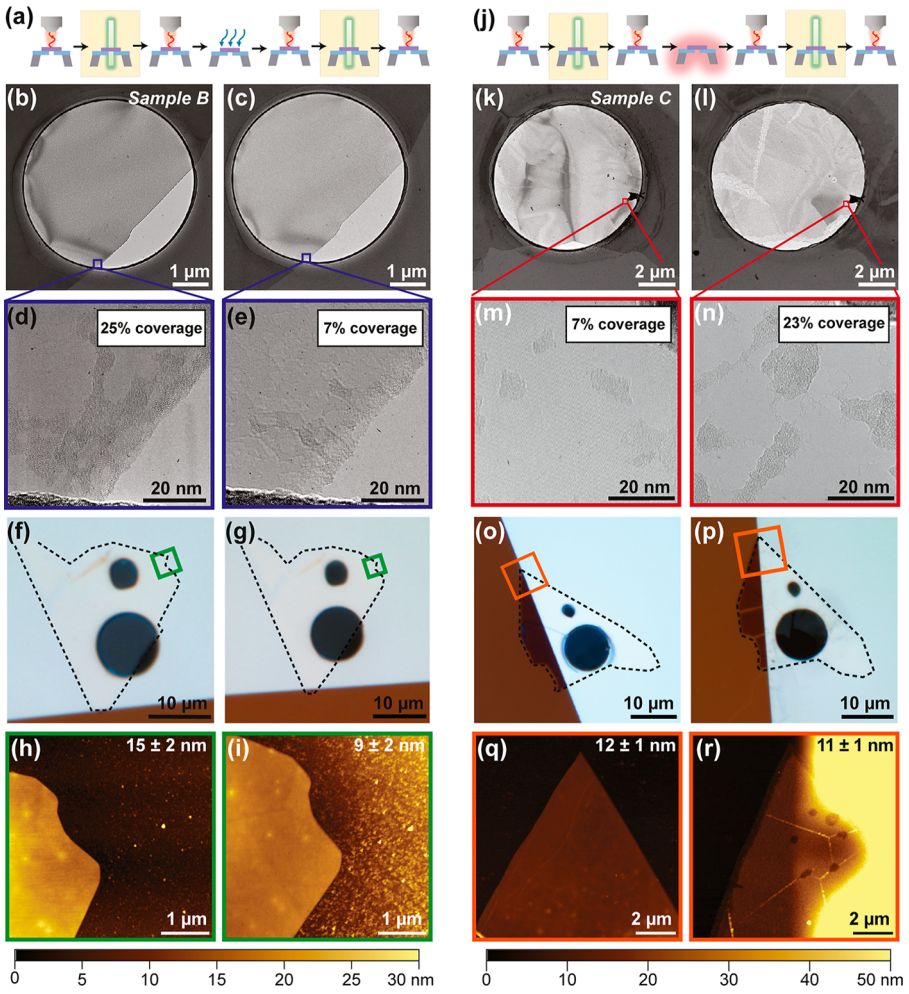

Figure 4. Effects of O_2 plasma on Sample B and annealing on Sample C, characterized by TEM and AFM. (a) Schematic representing the treatments and measurements performed on Sample B. The icons boxed in yellow correspond to the results included in subsequent panels. (b–e) TEM images of Sample B before and after oxygen plasma treatment. Navy boxes in (b,c) correspond to (d,e), respectively. (f,g) White light images before and after oxygen plasma treatment. Green boxes indicate AFM region. (h,i) AFM scans of Sample B before and after oxygen plasma treatment. (j) Schematic representing the series of treatments and measurements performed on Sample C. The icons boxed in yellow correspond to the results included in subsequent panels. (k–n) TEM images of Sample C before and after annealing. Red boxes in (k,l) correspond to (m,n), respectively. (o,p) White light images before and after annealing. Orange boxes indicate AFM region. (q,r) AFM scans of Sample C before and after annealing.

irradiated for ∼40 min—appears significantly dimmer. The brightening and shift from spatially localized to diffuse emission is consistent across other TEM-imaged samples in this study (Figure S10c,g), as well as findings in prior work.[26] The subsequent dimming with extended electron irradiation, however, is a notable exception to the trend. The non-monotonic change in optical activity may be related to the nonmonotonic changes in PDMS residue observed in the TEM images of Sample A. Previous authors have even proposed organic compounds as the source of visible emission in hBN.[42] It is also notable that the 80 kV accelerating voltage used here exceeds the knock-on energies of boron and nitrogen.[26,43−45] Therefore, the optical variations could reflect changes in chemical bonding of quantum emitters, or variations in hBN's Fermi level that affect the emitter charge states.

Emitter family analysis of the PL image taken after TEM measurements reveals the presence of two emitter groups in the darker region (Figure 3g). These groups may have evolved from those groups that were initially present before TEM irradiation (Figure 3d), however direct identification is unclear. The overall trend is a decrease in both the density and brightness of emitters, whereas the brightness level of uniform background PL has increased. Since the emitter family analysis assumes a random spatial distribution, it cannot be applied to the bright region of Figure 3f, because it exhibits a clear spatial gradient in brightness. The background level of this bright region, which may reflect a dense ensemble of emitters, is indicated in Figure 3g for reference. Meanwhile, the spatially averaged emission spectrum shows a shift toward longer wavelengths following electron irradiation (purple curve in Figure 3e). This is further evidence in support of changes to the nature of emitters due to TEM exposure, whether that be direct, e.g., through the creation of new emitters, or indirect, e.g., through modulation of the material's Fermi level or predominant optical relaxation pathways.

Treatment Effects. To investigate the effects of sample treatments on the hBN, we study separate samples in parallel using TEM and PL microscopy to decouple the effects of TEM on PL emission. We perform two treatments (oxygen plasma

https://doi.org/10.1021/acsnano.4c17676
ACS Nano 2025, 19, 11100−11110

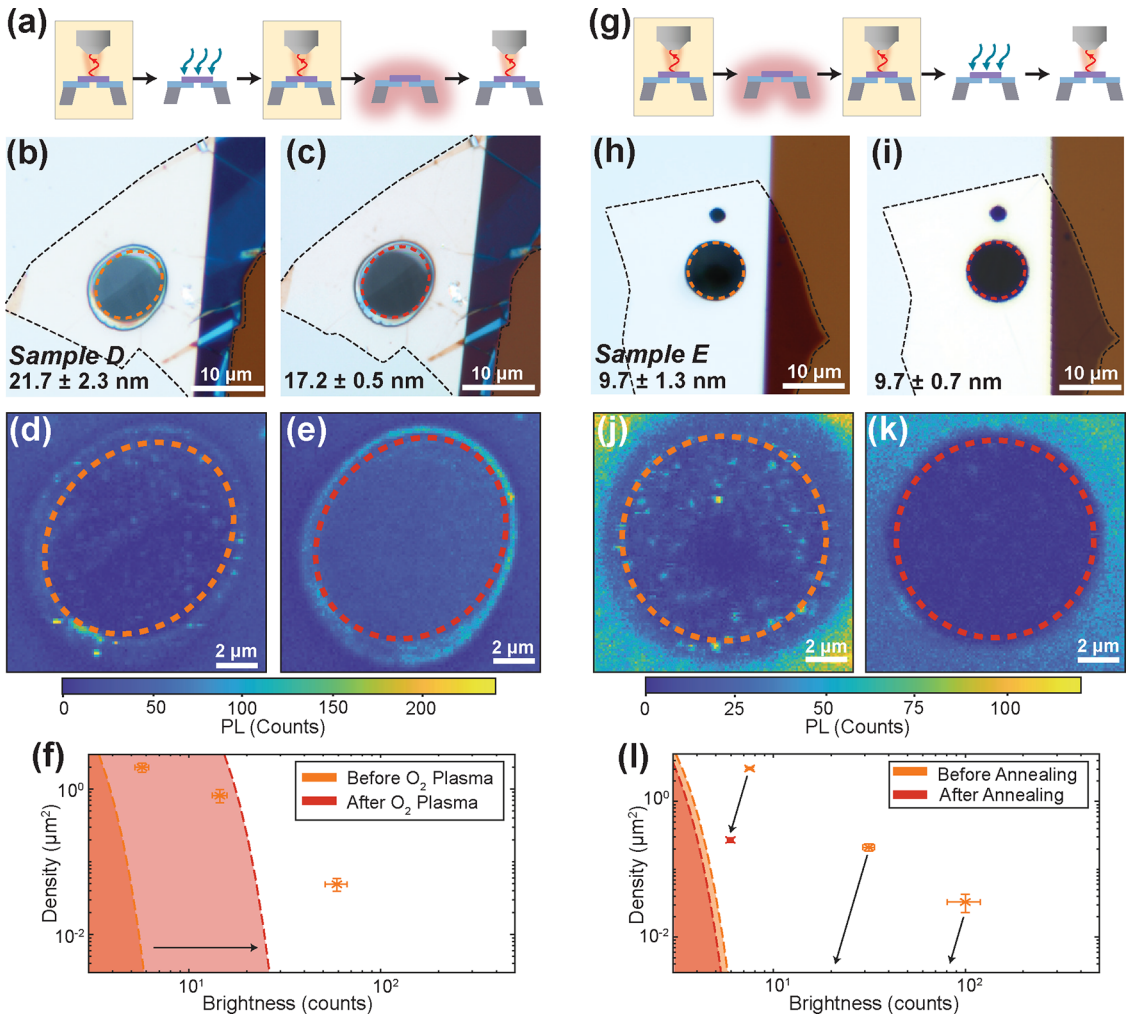

Figure 5. Effects of O_2 plasma on Sample D and annealing on Sample E, characterized by PL measurements. (a) Schematic representing the series of treatments and measurements performed on Sample D. The icons boxed in yellow correspond to the results included in subsequent panels. (b,c) White light images showing Sample D (hBN flake outlined in black) before (b) and after (c) oxygen plasma treatment. Orange and red dashed ovals outline the area suspended over the FIB hole. (d,e) PL images of Sample D before (d) and after (e) oxygen plasma treatment. Areas within orange and red dashed ovals are analyzed in (f). (f) Emitter family analysis of Sample D before and after oxygen plasma treatment. Arrow indicates the increase in background emission due to the treatment. (g) Schematic representing the series of treatments and measurements performed on Sample E. The icons boxed in yellow correspond to the results included in subsequent panels. (h,i) White light images showing Sample E (hBN flake outlined in black) before (h) and after (i) annealing. Orange and red dashed circles outline the area suspended over the FIB hole. (j,k) PL images of Sample E before (j) and after (k) annealing. Areas within orange and red dashed circles are analyzed in (l). (l) Emitter family analysis of Sample E before and after annealing. Arrows indicate a proposed evolution of the emitter families.

and annealing) on hBN and study the resulting optical and structural changes. Oxygen plasma and annealing are commonly used to improve quantum emission in hBN (e.g., increasing brightness and density of emitters),[6,21,31] but their effects on the morphology of the material are not well understood. In this section, we study four samples of hBN (Samples B through E). These samples are comparable in thickness (see Table S1) and were fabricated using identical protocols.

Figure 4 summarizes morphological changes to the exfoliated hBN flakes after oxygen plasma and annealing. Sample B was treated with oxygen plasma for 5 min (50 W, 50 sccm O_2). TEM images show that on the micron scale, this treatment smoothed wrinkles on the flake (Figure 4b,c) but had no other noticeable effects. On the nanometer scale, however, oxygen plasma significantly reduced contamination coverage on Sample B from 25% to 7%, with a similar decrease in average contaminant area size in the representative region analyzed (Figures 4d,e and S7). Furthermore, TEM images indicate that etching of hBN occurred, evidenced by the appearance of triangular-shaped defects following oxygen plasma treatment (Figure 4e). This treatment also resulted in significant thinning of Sample B ($15 \pm 2 \rightarrow 9 \pm 2$ nm) and a decrease in surface roughness by a factor of ~2 (see Tables S1 and S2 and Figures S2 and S3). These changes are consistent with the removal of surface contaminants along with etching of hBN. The former result was expected, given that oxygen plasma treatment is regularly employed as a cleaning method,[46−48] however ideally the treatment should not etch the hBN. The Supporting Information includes further data on Samples E and F, which were treated with oxygen plasma using a lower oxygen flow rate and longer time, indicating that the amount of etching can be reduced using these parameters.

https://doi.org/10.1021/acsnano.4c17676
ACS Nano 2025, 19, 11100−11110

In comparison, Sample C was annealed for 2 h at 850 °C in an argon environment. TEM images show that annealing resulted in significant cracking and warping of the flake (Figure 4k,l). Annealing also resulted in the formation of submicron holes, visible in the bottom right corner of Figure 4l and in the AFM data of Figure 4r. These changes may result from differing rates of thermal expansion between the hBN flake and the underlying SiN_x membrane.[49] Further analysis of TEM images reveal a local increase in contamination coverage (from 7% to 23%) and average contaminant size (from 18 to 56 nm^2) on Sample C (see Figures 4m,n and S8). This implies that the annealing treatment either augments contamination or, at minimum, induces a substantial redistribution of contaminants on the hBN surface. These changes are unexpected since annealing, like oxygen plasma, is often utilized as a cleaning technique.[50,51] AFM measurements of Sample C show that the annealing treatment results in a ∼2.5-fold increase in roughness without significant thinning (Figure 4q,r and Tables S1 and S2). PL images acquired at different stages of the experiment (Figure 4a,j) reflect the effects of TEM exposure as well as the treatments; these data are available in Figure S10 of the Supporting Information.

Figure 5 shows how comparable annealing and oxygen plasma treatments affect hBN's optical activity in the absence of TEM exposure. As indicated in Figure 5a,g, this figure focuses on the effects of these treatments individually. The results of the sequential treatments are shown in Figure S11 in the Supporting Information. Like Sample B, Sample D was exposed to oxygen plasma for 5 min (50 W, 50 sccm O_2). While there are no obvious changes visible in the white-light optical image, AFM reveals that the flake becomes thinner (Figure 5b,c). The initial PL image shows localized emission over the suspended region (Figure 5d), similar to other samples. After the oxygen plasma treatment, the PL becomes bright and diffuse without any localized emission visible (Figure 5d). Quantitative analysis uncovers three emitter families initially present in the sample (Figure 5f). After oxygen plasma treatment, a spatial gradient prevents analysis of the emitter families. However, we observe that the background level increases significantly.

The brightening and shift to a diffuse morphology observed in Sample D were unexpected since oxygen plasma treatments are typically used as a cleaning procedure.[52−54] However, these changes could be attributed to damage from etching or oxygen implantation. AFM measurements revealed that the sample is thinned (Table S1), and the treatment is the same as for Sample B, for which obvious evidence of etching was observed in TEM (Figure 4b−e). Potentially, damage from oxygen plasma treatment could increase the background brightness similarly to electron irradiation in the TEM. The effects differ, however, in that oxygen plasma primarily affects the material's surface, whereas electron irradiation can impact the bulk.[55] The majority of reports only consider oxygen plasma treatment followed by annealing, as it has been suggested that both treatments are necessary for stable emitter formation.[31] Another possible explanation for the increase in brightness is that oxygen ions are implanted during the irradiation process, changing hBN's chemical composition. Previous studies have shown that oxygen ion implantation can alter the optical properties of hBN, including a shift to a diffuse morphology.[32]

The Supporting Information includes further examples of changes in PL following oxygen plasma treatment of other samples (Figures S10 and S12). The samples consistently exhibited a shift to diffuse emission, however the changes in brightness were less consistent, indicating that the treatment does not affect all samples equally. Sample D exhibited the greatest increase in brightness. When using a lower oxygen flow rate for a longer time, we observed negligible changes to the PL characteristics (Figure S12) and less thinning in AFM (Figure S2). These observations highlight the future potential to tune the treatment recipe as required to achieve a desired outcome.

Sample E was annealed at 850 °C for 2 h in an argon environment, using the same procedure as for Sample C. After the treatment, the sample maintains its thickness and appears largely unchanged under white light, although slight variations in color that are apparent before annealing appear to diminish afterward (Figure 5h,i). AFM measurements show that the surface roughness of Sample E increased substantially upon annealing, consistent with the results of an identical annealing treatment applied to Sample C. Interestingly, Sample E was subjected to an oxygen plasma treatment (50 W, 25 sccm O_2, 10 min) following annealing, and yet the surface roughness remains more than twice as high as the pretreatment measurement. The initial PL image (Figure 5j) displays the same background pattern as its corresponding white light image (Figure 5h), superimposed with localized emitters. After the sample is annealed, however, few localized emitters remain, and they appear almost uniform with the background (Figure 5k). Emitter family analysis identifies three distinct groups before Sample E was annealed and only one group afterward, with negligible changes to the background (Figure 5l). The one remaining emitter group is dimmer than all of the groups from before the treatment. This result contrasts with previous studies, as annealing is regularly used to stabilize and brighten emitters in hBN.[6,21] In this case, emission becomes dimmer, and the few localized emitters that remain are unstable. These qualitative features are consistent across all samples observed in this study.

The thinness of the samples may help to explain the discrepancy, since prior works on quantum emitters in exfoliated hBN generally consider much thicker flakes (≳100 nm). Selection bias may play a role as well, since annealing's brightening effect might apply mainly to crystals that already host stable emitters, and samples without improved optical properties are excluded from such reports. If quantum emission arises from lattice defects, the decrease in PL intensity could correspond to annealing repairing the lattice. Even though the TEM image of Sample C shows global warping of the sample (Figure 4k,l), annealing would still be expected to heal the lattice on the local atomic scale. The suspended region of Sample C has no discernible PL signal after annealing, confirming that warping does not by itself induce brightening (Figure S10h). Another explanation for the dimming effect is defect migration or transmutation, which potentially reduces the density of emitters or blue-shifts their excitation or emission wavelength to become undetectable in our experimental setup.[28,56]

CONCLUSIONS AND OUTLOOK

In this work, we demonstrated a method for sequential, correlated TEM and PL measurements of multilayer hBN, and we used these complementary techniques, along with AFM and white light imaging, to study the interplay between surface contamination, overall morphology, flake thickness, and optical properties of mechanically exfoliated hBN—all critical

https://doi.org/10.1021/acsnano.4c17676
ACS Nano 2025, 19, 11100−11110

considerations toward scalable quantum information and photonics technologies utilizing hBN. We show that viscoelastic stamping with PDMS results in considerable residue on the surface of hBN flakes through direct TEM imaging and elemental mapping. We observe that the residue exhibits nonmonotonic changes in structure, and the optical emission exhibits nonmonotonic changes in brightness as a result of electron irradiation. In these samples, all optical emission is unstable and subject to photobleaching, potentially due to the flake thickness. We find that oxygen plasma treatment results in thinning of hBN and reduces surface residue while brightening and diffusing PL emission. In contrast, annealing induces warping and cracking in hBN flakes and results in an increase or redistribution of surface residue while reducing optical activity overall. These results contradict previous assumptions that such treatments clean the surface by removing residue without inflicting damage on the hBN, highlighting the need for further investigations of this subject.

Such work could include a systematic comparison of different sample preparation methods (i.e., dry transfer, wet transfer, etc.) and investigations of the resulting residue or lack thereof; a systematic comparison of the effect of thickness on optical activity, especially in combination with thermal annealing; fine-tuning of oxygen plasma parameters to optimally clean surfaces without damaging the hBN matrix; and investigation of large-scale morphological (e.g., strain-induced) effects by utilizing different sample substrates and geometries and annealing recipes. Motivated by the broad and interdisciplinary use of hBN, such studies can significantly advance the realization of new nanoelectronic and nanophotonic technologies. Likewise for use in quantum information science and photonics, quantitative understanding and control of surface contamination is essential to engineering materials and devices. By correlating optical and structural imaging, it will become possible to characterize and potentially even create quantum emitters at the atomic scale, facilitating the design and realization of new generations of quantum technologies based on hBN. Moreover, the methods and procedures introduced in this work can be directly adapted to study the structural and optical properties of a broad range of 2D materials.

METHODS

Sample Preparation. TEM grids were purchased from SiMPore with 50 nm-thick SiN_x membranes suspended above silicon supports. The suspended SiN_x region was 100 × 100 μm large. Holes of varying sizes (1- to 10-μm diameter) were drilled in the SiN membranes with a Xe^+ ion beam in a Tescan S8252X plasma focused ion beam scanning electron microscope (PFIB-SEM). The PFIB was operated at 15 kV and 300 pA for drilling and the SEM at 5 kV and 100 pA for imaging of SiN membranes. Once patterned with holes of the desired size and location, we mechanically exfoliated hBN (HQ Graphene) and transferred multilayer flakes onto the SiN membranes with PDMS stamping. This procedure has been previously reported; see Bhatia et al.[38] and Keneipp et al.[26] for more details.

Atomic Force Microscopy. AFM measurements were performed using a Bruker Icon AFM. To obtain values for flake thickness and roughness, regions of the flake comparable in thickness (as determined by white-light imaging) to the suspended region were scanned. In general, AFM scans improved when taken areas of the flake supported by the silicon substrate, instead of regions of the flake on the SiN_x membrane, as the thin SiN_x membrane resulted in a strong, nonuniform background signal in the AFM scans. Additional information about AFM data processing are provided in the Supporting Information.

Optical Characterization. PL images were collected using a custom-built confocal microscope with a 592 nm continuous-wave laser (MPB Communications, VF-P-200-592). The sample was illuminated with circularly polarized light at 100 μW unless otherwise noted. A long-pass filter with a cut-on wavelength of 650 nm (Semrock, BLP01-635R-25) is placed in the collection path to eliminate scattered light. The collected emission goes through a multimode fiber that is either routed to single-photon counting modules (Laser Components, Count T-100) or a spectrometer (Princeton Instruments, Iso-Plane160 and Pixis 100 CCD). For further details, see Patel et al.[9]

Emitter Family Analysis. The analysis used to categorize emitter groups is based on previous work by Breitweiser et al.[21] Briefly, we consider a histogram of the pixel intensity for selected regions of PL images (as indicated by dashed ovals in Figures 3 and 5). Fits of the histogram determine the background level and the properties of each emitter group. We select the number of emitter groups based on the reduced chi-squared value of the overall fit, and we extract density and brightness parameters from the emitter groups.

TEM Characterization. TEM characterization was performed in the JEOL JEM-F200 S/TEM equipped with a Gatan OneView Camera and JEOL dual SDD detectors for EDS spectra acquisition. The JEOL F200 was operated at 80 kV in both TEM mode and STEM mode. All TEM data were processed using Gatan Digital-Micrograph and ImageJ.

TEM Residue Analysis. TEM micrographs for Samples A, B and C were analyzed using an image processing routine to identify regions of residue on each flake. This image processing routine is described in detail in Sections SIV and SV of the Supporting Information. Once contaminated regions were identified, histograms of contaminated area size were plotted (see Figure 2e–g) to quantify the changes observed in TEM micrographs.

Sample Treatments. Oxygen plasma treatment was performed on hBN samples in an Anatech SCE 108 Barrel Asher. TEM grids with hBN flakes were secured to a 4-in., 500 μm Si and 1500 Å silicon oxide wafer using kapton tape. This wafer was placed into the process chamber with oxygen plasma at 50 W with flow rate of 25 or 50 sccm for 5 or 10 min, respectively.

Annealing treatment was performed on hBN samples in the Carbolite HZS 1200 °C 3 Zone Split Tube Furnace. The tube used is dedicated to hBN use only and cleaned prior to treatment with isopropyl alcohol and pressurized nitrogen gas. Samples are placed in an alumina ceramic boat and annealed in an Ar environment at 850 °C for 2 h.

ASSOCIATED CONTENT

Data Availability Statement

A preprint of this manuscript is also available: Gusdorff, J. A.; Bhatia, P.; Shin, T. T.; Uy-Tioco, A. S.; Sailors, B. N.; Keneipp, R. N.; Drndić, M.; Bassett, L. C. Correlated Structural and Optical Characterization of Hexagonal Boron Nitride. arXiv 2024, arXiv:2411.14408. https://arxiv.org/abs/2411.14408 (accessed on January 31, 2025).

Supporting Information

The Supporting Information is available free of charge at https://pubs.acs.org/doi/10.1021/acsnano.4c17676.

Details regarding sample processing, sample characterization, EDS mapping, contamination analysis, and additional optical characterization (PDF)

AUTHOR INFORMATION

Corresponding Authors

Marija Drndić − *Department of Physics and Astronomy, University of Pennsylvania, Philadelphia, Pennsylvania*

https://doi.org/10.1021/acsnano.4c17676
ACS Nano 2025, 19, 11100−11110

*19104, United States; orcid.org/0000-0002-8104-2231; Email: drndic@physics.upenn.edu

Lee C. Bassett − *Quantum Engineering Laboratory, Department of Electrical and Systems Engineering, University of Pennsylvania, Philadelphia, Pennsylvania 19104, United States;* orcid.org/0000-0001-8729-1530; Email: lbassett@seas.upenn.edu

Authors

Jordan A. Gusdorff − *Quantum Engineering Laboratory, Department of Electrical and Systems Engineering, University of Pennsylvania, Philadelphia, Pennsylvania 19104, United States; Department of Materials Science and Engineering, University of Pennsylvania, Philadelphia, Pennsylvania 19104, United States;* orcid.org/0000-0001-6609-2997

Pia Bhatia − *Department of Physics and Astronomy, University of Pennsylvania, Philadelphia, Pennsylvania 19104, United States;* orcid.org/0000-0001-6224-5933

Trey T. Shin − *Department of Materials Science and Engineering and Department of Physics and Astronomy, University of Pennsylvania, Philadelphia, Pennsylvania 19104, United States;* orcid.org/0000-0001-7494-8898

Alexandra Sofia Uy-Tioco − *Department of Materials Science and Engineering and Department of Physics and Astronomy, University of Pennsylvania, Philadelphia, Pennsylvania 19104, United States*

Benjamin N. Sailors − *Department of Physics and Astronomy and Department of Materials Science and Engineering, University of Pennsylvania, Philadelphia, Pennsylvania 19104, United States*

Rachael N. Keneipp − *Department of Physics and Astronomy, University of Pennsylvania, Philadelphia, Pennsylvania 19104, United States*

Complete contact information is available at: https://pubs.acs.org/10.1021/acsnano.4c17676

Author Contributions

‖J.A.G. and P.B. contributed equally.

Notes

The authors declare the following competing financial interest(s): Marija Drndic reports a consulting/advisory relationship with Goeppert, LLC.

ACKNOWLEDGMENTS

J.A.G. and L.C.B. acknowledge support from the NSF under awards DMR-1922278 and DMR-2019444. J.A.G. also acknowledges support from an NSF Graduate Research Fellowship (DGE-1845298). P.B., T.T.S., A.S.U.-T., B.N.S., R.N.K., and M.D. acknowledge support from DOE grant DE-SC0023224 on advanced in situ TEM analysis and ex situ studies of 2D hBN. P.B. was supported by NIH grant R01HG012413 for the development of hBN/graphene nanopores. This work was carried out in part at the Singh Center for Nanotechnology, which is supported by the NSF National Nanotechnology Coordinated Infrastructure Program under grant NNCI-2025608. The authors also acknowledge use of facilities and instrumentation supported by NSF through the University of Pennsylvania Materials Research Science and Engineering Center (MRSEC) (DMR-1720530). Finally, the authors also wish to thank D. Yates and J. Ford for their assistance with TEM characterization and FIB milling of substrates.

REFERENCES

(1) Shaik, A. B. D.; Palla, P. Optical Quantum Technologies with Hexagonal Boron Nitride Single Photon Sources. *Sci. Rep.* **2021**, *11*, 12285.

(2) Jungwirth, N. R.; Calderon, B.; Ji, Y.; Spencer, M. G.; Flatté, M. E.; Fuchs, G. D. Temperature Dependence of Wavelength Selectable Zero-Phonon Emission from Single Defects in Hexagonal Boron Nitride. *Nano Lett.* **2016**, *16*, 6052−6057.

(3) Dean, C. R.; Young, A. F.; Meric, I.; Lee, C.; Wang, L.; Sorgenfrei, S.; Watanabe, K.; Taniguchi, T.; Kim, P.; Shepard, K. L.; Hone, J. Boron Nitride Substrates for High-Quality Graphene Electronics. *Nat. Nanotechnol.* **2010**, *5*, 722−726.

(4) Yu, G. L.; Jalil, R.; Belle, B.; Mayorov, A. S.; Blake, P.; Schedin, F.; Morozov, S. V.; Ponomarenko, L. A.; Chiappini, F.; Wiedmann, S.; Zeitler, U.; Katsnelson, M. I.; Geim, A. K.; Novoselov, K. S.; Elias, D. C. Interaction Phenomena in Graphene Seen Through Quantum Capacitance. *Proc. Natl. Acad. Sci. U.S.A.* **2013**, *110*, 3282−3286.

(5) Kuiri, M.; Kumar, C.; Chakraborty, B.; Gupta, S. N.; Naik, M. H.; Jain, M.; Sood, A. K.; Das, A. Probing 2D Black Phosphorus by Quantum Capacitance Measurements. *Nanotechnology* **2015**, *26*, 485704.

(6) Tran, T. T.; Elbadawi, C.; Totonjian, D.; Lobo, C. J.; Grosso, G.; Moon, H.; Englund, D. R.; Ford, M. J.; Aharonovich, I.; Toth, M. Robust Multicolor Single Photon Emission from Point Defects in Hexagonal Boron Nitride. *ACS Nano* **2016**, *10*, 7331−7338.

(7) Exarhos, A. L.; Hopper, D. A.; Grote, R. R.; Alkauskas, A.; Bassett, L. C. Optical Signatures of Quantum Emitters in Suspended Hexagonal Boron Nitride. *ACS Nano* **2017**, *11*, 3328−3336.

(8) Mendelson, N.; Xu, Z. Q.; Tran, T. T.; Kianinia, M.; Scott, J.; Bradac, C.; Aharonovich, I.; Toth, M. Engineering and Tuning of Quantum Emitters in Few-Layer Hexagonal Boron Nitride. *ACS Nano* **2019**, *13*, 3132−3140.

(9) Patel, R. N.; Hopper, D. A.; Gusdorff, J. A.; Turiansky, M. E.; Huang, T.-Y.; Fishman, R. E. K.; Porat, B.; Van de Walle, C. G.; Bassett, L. C. Probing the Optical Dynamics of Quantum Emitters in Hexagonal Boron Nitride. *PRX Quantum* **2022**, *3*, 030331.

(10) Exarhos, A. L.; Hopper, D. A.; Patel, R. N.; Doherty, M. W.; Bassett, L. C. Magnetic-Field-Dependent Quantum Emission in Hexagonal Boron Nitride at Room Temperature. *Nat. Commun.* **2019**, *10*, 222.

(11) Chejanovsky, N.; Mukherjee, A.; Geng, J.; Chen, Y. C.; Kim, Y.; Denisenko, A.; Finkler, A.; Taniguchi, T.; Watanabe, K.; Dasari, D. B. R.; Auburger, P.; Gali, A.; Smet, J. H.; Wrachtrup, J. Single-Spin Resonance in a Van der Waals Embedded Paramagnetic Defect. *Nat. Mater.* **2021**, *20*, 1079−1084.

(12) Guo, N. J.; Li, S.; Liu, W.; Yang, Y. Z.; Zeng, X. D.; Yu, S.; Meng, Y.; Li, Z. P.; Wang, Z. A.; Xie, L. K.; Ge, R. C.; Wang, J. F.; Li, Q.; Xu, J. S.; Wang, Y. T.; Tang, J. S.; Gali, A.; Li, C. F.; Guo, G. C. Coherent Control of an Ultrabright Single Spin in Hexagonal Boron Nitride at Room Temperature. *Nat. Commun.* **2023**, *14*, 2893.

(13) Patel, R. N.; Fishman, R. E.; Huang, T. Y.; Gusdorff, J. A.; Fehr, D. A.; Hopper, D. A.; Breitweiser, S. A.; Porat, B.; Flatté, M. E.; Bassett, L. C. Room Temperature Dynamics of an Optically Addressable Single Spin in Hexagonal Boron Nitride. *Nano Lett.* **2024**, *24*, 7623−7628.

(14) Stern, H. L.; Gilardoni, C. M.; Gu, Q.; Eizagirre Barker, S.; Powell, O. F. J.; Deng, X.; Fraser, S. A.; Follet, L.; Li, C.; Ramsay, A. J.; Tan, H. H.; Aharonovich, I.; Atatüre, M. A Quantum Coherent Spin in Hexagonal Boron Nitride at Ambient Conditions. *Nat. Mater.* **2024**, *23*, 1379−1385.

(15) Akbari, H.; Lin, W. H.; Vest, B.; Jha, P. K.; Atwater, H. A. Temperature-dependent Spectral Emission of Hexagonal Boron Nitride Quantum Emitters on Conductive and Dielectric Substrates. *Phys. Rev. Appl.* **2021**, *15*, 014036.

(16) Proscia, N. V.; Shotan, Z.; Jayakumar, H.; Reddy, P.; Cohen, C.; Dollar, M.; Alkauskas, A.; Doherty, M.; Meriles, C. A.; Menon, V. M. Near-Deterministic Activation of Room-Temperature Quantum Emitters in Hexagonal Boron Nitride. *Optica* **2018**, *5*, 1128−1134.

(17) Sajid, A.; Thygesen, K. S. VNCB Defect as Source of Single Photon Emission from Hexagonal Boron Nitride. *2D Materials* **2020**, *7*, 031007.
(18) Yang, F.; Stando, G.; Thompson, A.; Gundurao, D.; Li, L.; Liu, H. Effect of Environmental Contaminants on the Interfacial Properties of Two-Dimensional Materials. *Acc. Mater. Res.* **2022**, *3*, 1022−1032.
(19) Li, S. X.; Ichihara, T.; Park, H.; He, G.; Kozawa, D.; Wen, Y.; Koman, V. B.; Zeng, Y.; Kuehne, M.; Yuan, Z.; Faucher, S.; Warner, J. H.; Strano, M. S. Prolonged Photostability in Hexagonal Boron Nitride Quantum Emitters. *Commun. Mater.* **2023**, *4*, 19.
(20) Wigger, D.; Schmidt, R.; Del Pozo-Zamudio, O.; Preuß, J. A.; Tonndorf, P.; Schneider, R.; Steeger, P.; Kern, J.; Khodaei, Y.; Sperling, J.; De Vasconcellos, S. M.; Bratschitsch, R.; Kuhn, T. Phonon-Assisted Emission and Absorption of Individual Color Centers in Hexagonal Boron Nitride. *2D Materials* **2019**, *6*, 035006.
(21) Breitweiser, S. A.; Exarhos, A. L.; Patel, R. N.; Saouaf, J.; Porat, B.; Hopper, D. A.; Bassett, L. C. Efficient Optical Quantification of Heterogeneous Emitter Ensembles. *ACS Photonics* **2020**, *7*, 288−295.
(22) Fournier, C.; Plaud, A.; Roux, S.; Pierret, A.; Rosticher, M.; Watanabe, K.; Taniguchi, T.; Buil, S.; Quélin, X.; Barjon, J.; Hermier, J. P.; Delteil, A. Position-Controlled Quantum Emitters with Reproducible Emission Wavelength in Hexagonal Boron Nitride. *Nat. Commun.* **2021**, *12*, 3779.
(23) Hayee, F.; Yu, L.; Zhang, J. L.; Ciccarino, C. J.; Nguyen, M.; Marshall, A. F.; Aharonovich, I.; Vučković, J.; Narang, P.; Heinz, T. F.; Dionne, J. A. Revealing Multiple Classes of Stable Quantum Emitters in Hexagonal Boron Nitride with Correlated Optical and Electron Microscopy. *Nat. Mater.* **2020**, *19*, 534−539.
(24) Alem, N.; Erni, R.; Kisielowski, C.; Rossell, M. D.; Gannett, W.; Zettl, A. Atomically Thin Hexagonal Boron Nitride Probed by Ultrahigh-Resolution Transmission Electron Microscopy. *Phys. Rev. B* **2009**, *80*, 155425.
(25) Bui, T. A.; Leuthner, G. T.; Madsen, J.; Monazam, M. R. A.; Chirita, A. I.; Postl, A.; Mangler, C.; Kotakoski, J.; Susi, T. Creation of Single Vacancies in hBN with Electron Irradiation. *Small* **2023**, *19*, 2301926.
(26) Keneipp, R. N.; Gusdorff, J. A.; Bhatia, P.; Shin, T. T.; Bassett, L. C.; Drndić, M. Nanoscale Sculpting of Hexagonal Boron Nitride with an Electron Beam. *J. Phys. Chem. C* **2024**, *128*, 8741−8749.
(27) Li, C.; Xu, Z.-Q.; Mendelson, N.; Kianinia, M.; Toth, M.; Aharonovich, I. Purification of Single-Photon Emission from hBN Using Post-Processing Treatments. *Nanophotonics* **2019**, *8*, 2049−2055.
(28) Venturi, G.; Chiodini, S.; Melchioni, N.; Janzen, E.; Edgar, J. H.; Ronning, C.; Ambrosio, A. Selective Generation of Luminescent Defects in Hexagonal Boron Nitride. *Laser Photonics Rev.* **2024**, *18*, 2300973.
(29) Mohajerani, S. S.; Chen, S.; Alaei, A.; Chou, T.; Liu, N.; Ma, Y.; Xiao, L.; Lee, S. S.; Yang, E.-H.; Strauf, S. Narrowband Quantum Light Emission from Oxygen-Related Color Centers in Hexagonal Boron Nitride. *ACS Photonics* **2024**, *11*, 2359−2367.
(30) Chen, Y.; Gale, A.; Yamamura, K.; Horder, J.; Condos, A.; Watanabe, K.; Taniguchi, T.; Toth, M.; Aharonovich, I. Annealing of Blue Quantum Emitters in Carbon-Doped Hexagonal Boron Nitride. *Appl. Phys. Lett.* **2023**, *123*, 041902.
(31) Fischer, M.; Caridad, J. M.; Sajid, A.; Ghaderzadeh, S.; Ghorbani-Asl, M.; Gammelgaard, L.; Bøggild, P.; Thygesen, K. S.; Krasheninnikov, A. V.; Xiao, S.; Wubs, M.; Stenger, N. Controlled Generation of Luminescent Centers in Hexagonal Boron Nitride by Irradiation Engineering. *Sci. Adv.* **2021**, *7*, No. eabe7138.
(32) Mendelson, N.; Chugh, D.; Reimers, J. R.; Cheng, T. S.; Gottscholl, A.; Long, H.; Mellor, C. J.; Zettl, A.; Dyakonov, V.; Beton, P. H.; Novikov, S. V.; Jagadish, C.; Tan, H. H.; Ford, M. J.; Toth, M.; Bradac, C.; Aharonovich, I. Identifying Carbon as the Source of Visible Single-Photon Emission from Hexagonal Boron Nitride. *Nat. Mater.* **2021**, *20*, 321−328.
(33) Tran, T. T.; Bray, K.; Ford, M. J.; Toth, M.; Aharonovich, I. Quantum Emission from Hexagonal Boron Nitride Monolayers. *Nat. Nanotechnol.* **2016**, *11*, 37−41.
(34) Ngoc My Duong, H.; Nguyen, M. A. P.; Kianinia, M.; Ohshima, T.; Abe, H.; Watanabe, K.; Taniguchi, T.; Edgar, J. H.; Aharonovich, I.; Toth, M. Effects of High-Energy Electron Irradiation on Quantum Emitters in Hexagonal Boron Nitride. *ACS Appl. Mater. Interfaces* **2018**, *10*, 24886−24891.
(35) Egerton, R.; Li, P.; Malac, M. Radiation Damage in the TEM and SEM. *Micron* **2004**, *35*, 399−409.
(36) Rykaczewski, K.; White, W. B.; Fedorov, A. G. Analysis of Electron Beam Induced Deposition (EBID) of Residual Hydrocarbons in Electron Microscopy. *J. Appl. Phys.* **2007**, *101*, No. eabe7138.
(37) Egerton, R. Radiation Damage to Organic and Inorganic Specimens in the TEM. *Micron* **2019**, *119*, 72−87.
(38) Bhatia, P.; Shin, T. T.; Kavetsky, K.; Sailors, B. N.; Siokos, G.; Uy-Tioco, A. S.; Keneipp, R. N.; Gusdorff, J. A.; Bassett, L. C.; Drndić, M. A Tale of Two Transfers: Characterizing Polydimethylsiloxane Viscoelastic Stamping and Heated Poly Bis-A Carbonate Transfer of Hexagonal Boron Nitride. *Micron* **2025**, *189*, 103747.
(39) Cheliotis, I.; Zergioti, I. A Review on Transfer Methods of Two-Dimensional Materials. *2D Materials* **2024**, *11*, 022004.
(40) Jain, A.; Bharadwaj, P.; Heeg, S.; Parzefall, M.; Taniguchi, T.; Watanabe, K.; Novotny, L. Minimizing Residues and Strain in 2D Materials Transferred from PDMS. *Nanotechnology* **2018**, *29*, 265203.
(41) Jang, D. J.; Haidari, M. M.; Kim, J. H.; Ko, J.-Y.; Yi, Y.; Choi, J. S. A Modified Wet Transfer Method for Eliminating Interfacial Impurities in Graphene. *Nanomaterials* **2023**, *13*, 1494.
(42) Neumann, M.; Wei, X.; Morales-Inostroza, L.; Song, S.; Lee, S. G.; Watanabe, K.; Taniguchi, T.; Götzinger, S.; Lee, Y. H. Organic Molecules as Origin of Visible-Range Single Photon Emission from Hexagonal Boron Nitride and Mica. *ACS Nano* **2023**, *17*, 11679−11691.
(43) Kotakoski, J.; Jin, C. H.; Lehtinen, O.; Suenaga, K.; Krasheninnikov, A. V. Electron Knock-on Damage in Hexagonal Boron Nitride Monolayers. *Phys. Rev. B* **2010**, *82*, 113404.
(44) Dai, C.; Popple, D.; Su, C.; Park, J.-H.; Watanabe, K.; Taniguchi, T.; Kong, J.; Zettl, A. Evolution of Nanopores in Hexagonal Boron Nitride. *Commun. Chem.* **2023**, *6*, 108.
(45) Gilbert, S. M.; Dunn, G.; Azizi, A.; Pham, T.; Shevitski, B.; Dimitrov, E.; Liu, S.; Aloni, S.; Zettl, A. Fabrication of Subnanometer-Precision Nanopores in Hexagonal Boron Nitride. *Sci. Rep.* **2017**, *7*, 15096.
(46) Na, Y. S.; Kim, J. H.; Kang, S.; Jeong, J. H.; Park, S.; Kim, D. H.; Ihm, K.; Watanabe, K.; Taniguchi, T.; Kwon, Y.-K.; Kim, Y. D.; Lee, G.-H. Modulation of Optical and Electrical Properties in Hexagonal Boron Nitride by Defects Induced via Oxygen Plasma Treatment. *2D Materials* **2021**, *8*, 045041.
(47) Jadwiszczak, J.; Kelly, D. J.; Guo, J.; Zhou, Y.; Zhang, H. Plasma Treatment of Ultrathin Layered Semiconductors for Electronic Device Applications. *ACS Appl. Electron. Mater.* **2021**, *3*, 1505−1529.
(48) Kim, S.; Choi, M. S.; Qu, D.; Ra, C. H.; Liu, X.; Kim, M.; Song, Y. J.; Yoo, W. J. Effects of Plasma Treatment on Surface Properties of Ultrathin Layered MoS2. *2D Materials* **2016**, *3*, 035002.
(49) Zhang, G.; Chang, Y.; Yan, B. The Study of the Wrinkles of Hexagonal Boron-Nitride Flake after the Annealing. *Crystals* **2023**, *13*, 304.
(50) Garcia, A. G. F.; Neumann, M.; Amet, F.; Williams, J. R.; Watanabe, K.; Taniguchi, T.; Goldhaber-Gordon, D. Effective Cleaning of Hexagonal Boron Nitride for Graphene Devices. *Nano Lett.* **2012**, *12*, 4449−4454.
(51) Lin, Y.-C.; Lu, C.-C.; Yeh, C.-H.; Jin, C.; Suenaga, K.; Chiu, P.-W. Graphene Annealing: How Clean Can It Be? *Nano Lett.* **2012**, *12*, 414−419.
(52) Griffiths, A. J. V.; Walther, T. Quantification of Carbon Contamination Under Electron Beam Irradiation in a Scanning Transmission Electron Microscope and its Suppression by Plasma Cleaning. *J. Phys.: Conf. Ser.* **2010**, *241*, 012017.

https://doi.org/10.1021/acsnano.4c17676
ACS Nano 2025, 19, 11100−11110

(53) Hugenschmidt, M.; Adrion, K.; Marx, A.; Müller, E.; Gerthsen, D. Electron-Beam-Induced Carbon Contamination in STEM-in-SEM: Quantification and Mitigation. *Microsc. Microanal.* **2023**, *29*, 219−234.
(54) Mitchell, D. Contamination Mitigation Strategies for Scanning Transmission Electron Microscopy. *Micron* **2015**, *73*, 36−46.
(55) Vogl, T.; Doherty, M. W.; Buchler, B. C.; Lu, Y.; Lam, P. K. Atomic Localization of Quantum Emitters in Multilayer Hexagonal Boron Nitride. *Nanoscale* **2019**, *11*, 14362−14371.
(56) Weston, L.; Wickramaratne, D.; Mackoit, M.; Alkauskas, A.; Van De Walle, C. G. Native Point Defects and Impurities in Hexagonal Boron Nitride. *Phys. Rev. B* **2018**, *97*, 214104.

https://doi.org/10.1021/acsnano.4c17676
ACS Nano 2025, 19, 11100−11110